

OPEN ACCESS

EDITED BY
Dianning He,
China Medical University, China

REVIEWED BY
Xiaojie Gan,
The First Affiliated Hospital of Soochow
University, China
Jiaying Li,
Zhejiang Hospital of Traditional Chinese
Medicine. China

*CORRESPONDENCE

Lei Han

Manlei1974@sina.com

Weng Kung Peng

peng.weng.kung.qiqb@osaka-u.ac.jp

[†]These authors have contributed equally to

[†]These authors have contributed equally to this work and share first authorship

RECEIVED 25 June 2025 ACCEPTED 17 October 2025 PUBLISHED 10 November 2025

CITATION

Wu J, Zuo ZD, Na L, Zhang W, Guo Y, Zhu ZW, Ren QY, Peng WK and Han L (2025) Machine learning-driven prediction of intratumoral tertiary lymphoid structures in hepatocellular carcinoma using contrast-enhanced CT imaging and integrated clinical data. *Front. Oncol.* 15:1652509. doi: 10.3389/fonc.2025.1652509

COPYRIGHT

© 2025 Wu, Zuo, Na, Zhang, Guo, Zhu, Ren, Peng and Han. This is an open-access article distributed under the terms of the Creative Commons Attribution License (CC BY). The use, distribution or reproduction in other forums is permitted, provided the original author(s) and the copyright owner(s) are credited and that the original publication in this journal is cited, in accordance with accepted academic practice. No use, distribution or reproduction is permitted which does not comply with these terms.

Machine learning-driven prediction of intratumoral tertiary lymphoid structures in hepatocellular carcinoma using contrast-enhanced CT imaging and integrated clinical data

Jun Wu^{1‡}, Zhifan Zuo^{2‡}, Lin Na^{3‡}, Wei Zhang¹, Yang Guo¹, Ziwei Zhu¹, Qiongyuan Ren⁴, Weng Kung Peng^{5*†} and Lei Han^{1*†}

¹Department of Hepatobiliary Surgery, The General Hospital of Northern Theater Command, Shenyang, Liaoning, China, ²Gynecological Radiotherapy Ward, Liaoning Provincial Cancer Hospital, Shenyang, Liaoning, China, ³Department of Central Laboratory, The First Affiliated Hospital of China Medical University, Shenyang, Liaoning, China, ⁴Dalian Medical University, The General Hospital of Northern Theater Command Training Base for Graduate, Shenyang, Liaoning, China, ⁵Center for Quantum Information and Quantum Biology, Institute of Advanced Co-Creation Studies, The University of Osaka, Osaka, Japan

Purpose: We developed a machine learning framework to predict the presence of tertiary lymphoid structures (TLSs) within tumors in patients with hepatocellular carcinoma (HCC). This framework uses computed tomography (CT) imaging and clinical data collected before surgery, providing a noninvasive method for prediction.

Methods: We conducted a retrospective analysis of HCC patients who underwent surgery at the General Hospital of the Northern Theater Command's Hepatobiliary Surgery Department between January 2017 and October 2024. Using Python software, we extracted radiomic features from preoperative CT images (arterial and portal venous phases). We then selected features associated with intratumoral TLSs using statistical methods, including intraclass correlation coefficient (ICC), Pearson correlation, t-tests, and LASSO regression. Three models were developed—clinical, radiomics, and combined—using machine learning techniques and independent clinical predictors. A predictive nomogram was created and evaluated using the area under the ROC curve (AUC) and calibration analysis.

Results: Our study included 171 HCC patients, with 80 showing negative and 91 showing positive expression of intratumoral TLSs. Multivariate analysis identified the albumin-bilirubin (ALBI) score as an independent predictor of intratumoral TLSs expression. The combined model demonstrated the highest predictive accuracy, with AUCs of 0.947 in the training set and 0.909 in the validation set, outperforming both the clinical (AUC: 0.709 training, 0.714 validation) and radiomics (AUC: 0.935 training, 0.890 validation) models.

Conclusion: Our combined machine learning model, which integrates preoperative CT imaging and clinical data, provides an accurate, noninvasive method for assessing intratumoral TLSs expression in HCC. This tool has the potential to enhance clinical decision-making, guide therapeutic planning, and facilitate personalized treatment strategies for HCC patients.

KEYWORDS

hepatocellular carcinoma, intratumoral tertiary lymphoid structures, machine learning, radiomics, contrast-enhanced CT

Introduction

Hepatocellular carcinoma (HCC) constitutes the predominant subtype of liver cancer, accounting for 75–85% of cases (1). Globally, it ranks as the sixth most commonly diagnosed malignancy and the third leading cause of cancer-related mortality (2). Although radical liver resection represents the primary curative treatment for HCC (3), most patients are diagnosed at intermediate or advanced stages, rendering them ineligible for surgical intervention (4). The heterogeneous nature of HCC, combined with its resistance to conventional radiotherapy and chemotherapy, contributes to a poor overall prognosis (5, 6).

Recent progress in targeted therapies and immunotherapies has introduced novel therapeutic options for HCC management. Immune checkpoint inhibitors, particularly those targeting programmed death-1 (PD-1) and cytotoxic T lymphocyte-associated antigen-4 (CTLA-4), have emerged as critical components of contemporary HCC research (7, 8). In a phase III clinical trial, nivolumab monotherapy achieved an objective response rate of 18.3% in patients with advanced HCC, demonstrating clinical efficacy and a favorable safety profile (9). Despite its superior efficacy relative to other treatments, immunotherapy is limited by significant interpatient variability in response (10). Consequently, the development of predictive biomarkers for immunotherapy response remains essential for optimizing clinical decision-making in HCC.

Tertiary lymphoid structures (TLSs) have recently emerged as a promising focus in cancer immunotherapy research due to their potential to improve treatment outcomes (11). These organized aggregates of immune cells develop in non-lymphoid tissues, driven by chronic inflammatory conditions such as cancer, autoimmune disorders, or persistent infections (12). Structurally, TLSs recapitulate the architecture of lymph nodes, featuring a core of B cells (CD20+) surrounded by T cells (CD3+), which collectively facilitate the initiation and coordination of adaptive immune responses (13). TLSs can remodel the local immune landscape by promoting the infiltration of anti-tumor effector cells while simultaneously suppressing pro-tumorigenic populations (14). This evidence positions TLSs as localized hubs for priming anti-tumor immunity, underscoring their significance as a key area of investigation for advancing therapeutic strategies.

Emerging evidence highlights the pivotal role of TLSs as central hubs for initiating systemic antitumor immune responses. In melanoma, dense perivascular clusters of CD8+ T cells surrounding TLSs underscore their function as activation sites for tumor-directed immunity (15). Mature TLSs have been identified as a key biomarker for predicting immunotherapy efficacy (16), with soft tissue sarcomas harboring TLSs exhibiting superior responses to immune checkpoint blockade (17). Clinically, TLSs presence correlates with prolonged overall survival across diverse malignancies, including gastric, cervical, and breast cancers (18-22). In HCC, intratumoral TLSs are linked to reduced early recurrence post-resection and better prognosis in early-stage disease (23). Furthermore, the spatial distribution and density of TLSs in intrahepatic cholangiocarcinoma offer a refined immune-based stratification system for prognostic assessment (24). Given these findings, preoperative prediction of TLSs presence in HCC holds significant clinical value, enabling more accurate prognosis estimation, personalized therapeutic strategies, and optimized treatment selection.

Currently, TLSs can only be definitively identified through postoperative histopathological analysis. However, HCC is primarily diagnosed non-invasively using imaging techniques such as computed tomography (CT) or magnetic resonance imaging (MRI), which often eliminates the need for pathological confirmation. Given the prognostic and therapeutic significance of TLSs, there is an urgent need for a non-invasive, efficient preoperative tool to predict the presence of intratumoral TLSs in HCC.

Machine learning (ML) has emerged as a powerful tool for disease diagnosis and treatment optimization, combining high accuracy with computational efficiency (25). Radiomics—a field focused on extracting and analyzing quantitative imaging features to uncover hidden biological patterns—has gained significant traction in clinical research due to its potential to predict disease onset, progression, and outcomes (26, 27). In liver cancer, radiomics has already demonstrated promising results. For instance, Feng et al. developed an MRI-based radiomics model for the preoperative prediction of microvascular invasion (MVI), achieving an area under the curve (AUC) of 0.83 (28). Similarly, Li et al. constructed a multiparametric CT-derived radiomics nomogram to identify the massive macrotrabecular HCC subtype with high accuracy (29).

Building on these advances, this study focuses on intratumoral TLSs in HCC and aims to develop a preoperative prediction model using machine learning algorithms applied to contrast-enhanced CT imaging and clinical data. The model is designed to improve clinical decision-making, advance precision medicine, enable personalized preoperative risk stratification, and optimize therapeutic strategies for HCC patients.

Materials and methods

bilirubin: RS. Rad Signature

Workflow for the development of the clinical-radiomics model is shown in Figure 1.

Data preparation and patient selection

The Ethics Committee of Northern Theater General Hospital approved this retrospective study conducted at a single center (Ethics No: Y(2024)028). Between 2017 and 2024, 353 consecutive HCC patients who underwent surgical treatment at the Hepatobiliary Surgery Department of Northern Theater General Hospital were included. The inclusion criteria were: (1) a confirmed postoperative pathological diagnosis of HCC; and (2) contrast-enhanced CT of the liver performed within 1 month before surgery. The exclusion criteria were: (1) lesion size <1.0 cm; (2) missing imaging or clinical data; (3) poor image quality that hindered lesion identification; (4) history of preoperative treatments such as radiotherapy, chemotherapy, targeted therapy, or immunotherapy; and (5) missing postoperative

pathological data (Figure 2). After applying the inclusion and exclusion criteria.

Baseline data collected included age, sex, hepatitis virus infection, Barcelona Clinic Liver Cancer staging (30), liver cirrhosis status (31), presurgical blood panels, clotting function, hepatic biochemical markers, albumin-bilirubin (ALBI) score, and serum AFP levels at admission. The calculation method for the ALBI score is provided in the Supplementary Material.

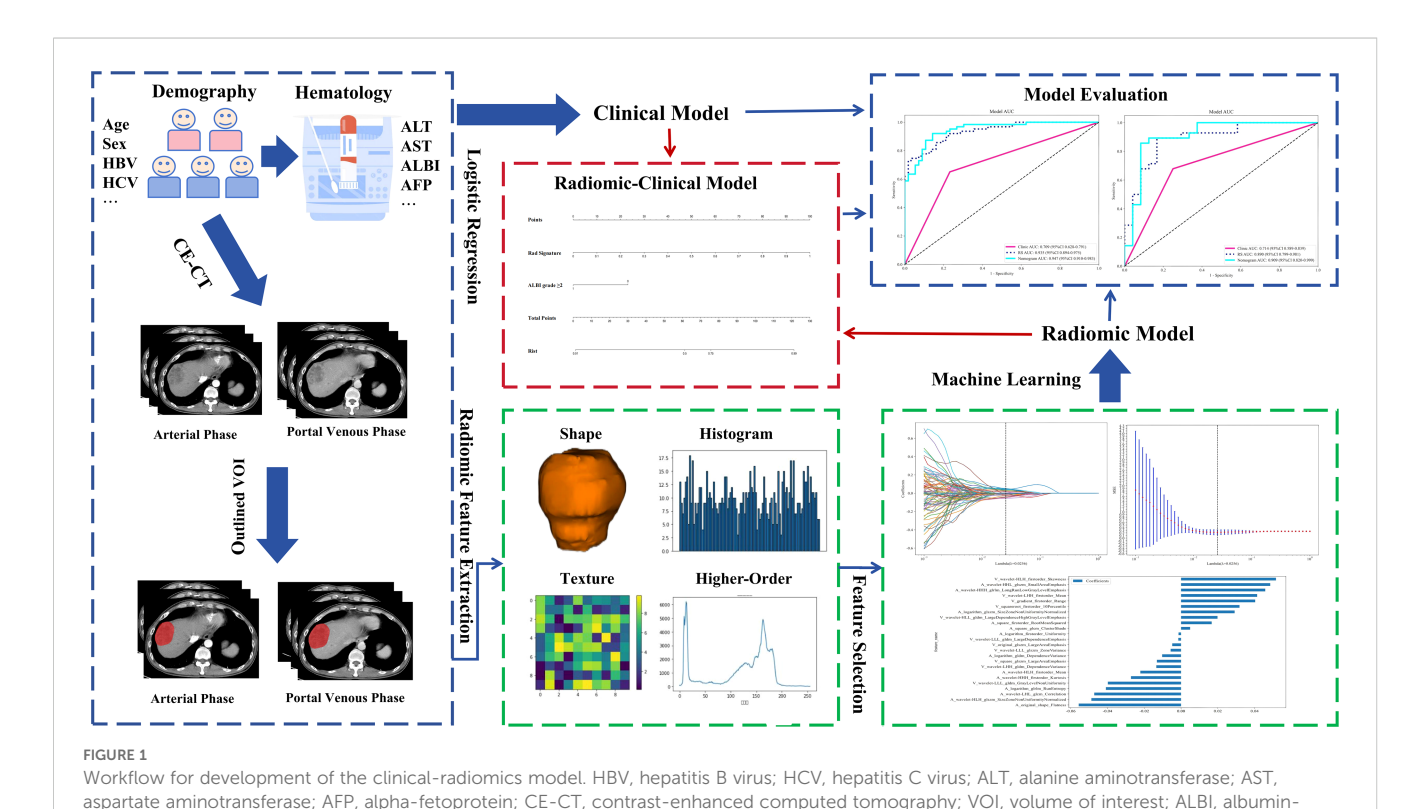
Pathological diagnosis

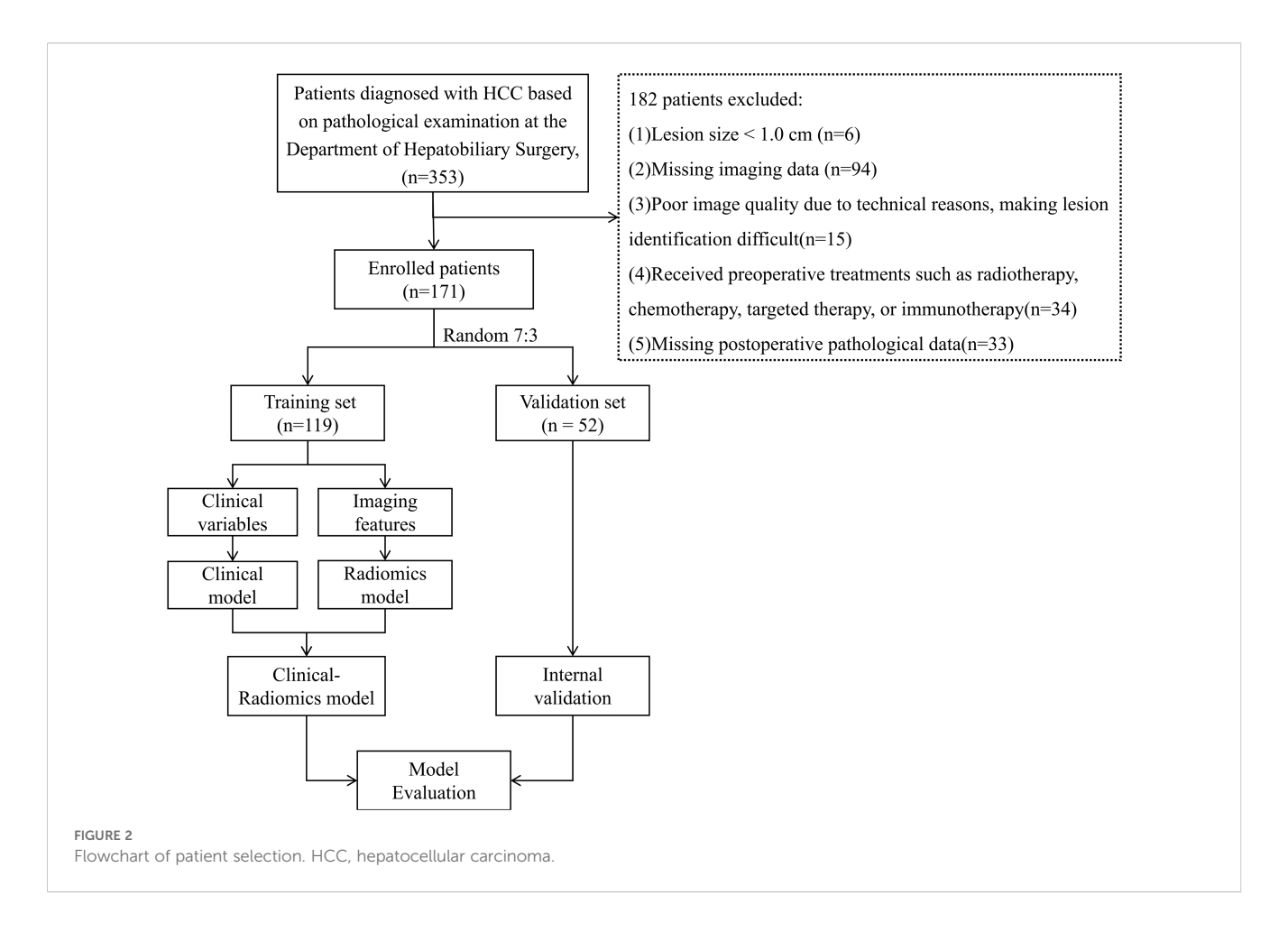
All tissue sections were reviewed by two pathologists, each with > 5 years of experience in liver pathology. The presence of intratumoral TLSs was morphologically assessed using H&E-stained histopathological slides. Any disagreements between the two pathologists were resolved by a third senior pathologist (associate chief or higher). Intratumoral TLSs were classified into two maturity stages: lymphoid aggregates (Agg) and lymphoid follicles (FOL) (17). Our analysis strictly adhered to the established classification and diagnostic criteria for intratumoral TLSs proposed by Julien Calderaro and colleagues (23).

Aggregates: Vague, ill-defined clusters of lymphocytes.

Primary follicles (FL-I) are round, well-defined clusters of lymphocytes without a germinal center. Secondary follicles (FL-II) are follicles that contain a visible germinal center.

Tumors containing at least one intratumoral TLS were classified as TLSs-positive, while those without were classified as TLSs-negative.





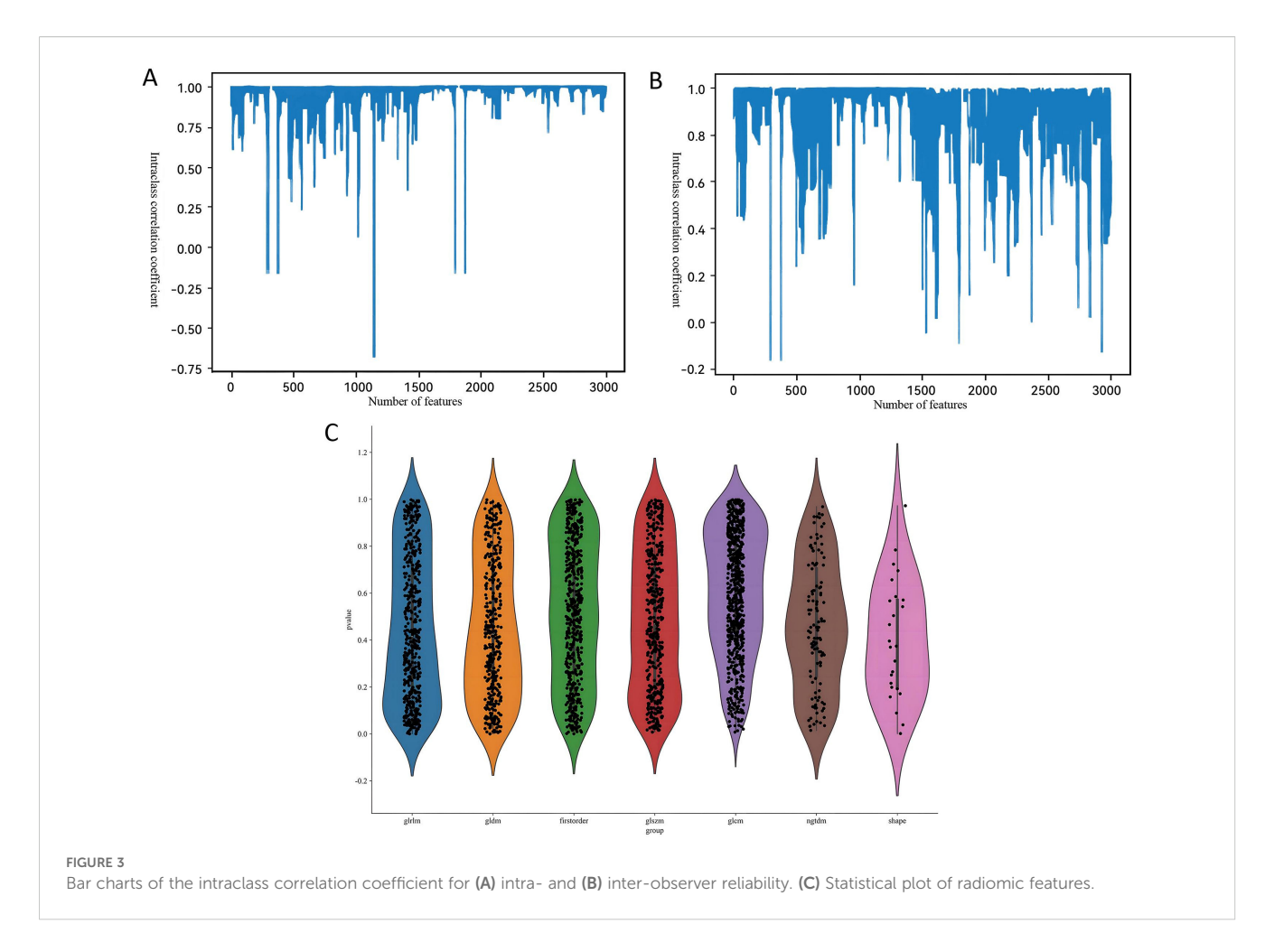
CT image acquisition, volume of interest segmentation, and extraction of radiological features

The process of CT image acquisition is detailed in the supplementary document. The images were imported into ITK-SNAP (version 3.8.0). An experienced physician specializing in abdominal imaging manually delineated the VOI for each tumor layer along the tumor boundaries using ITK-SNAP. Before model construction, imaging data from 20 randomly selected patients were used. The first physician reoutlined the VOI after 1 month. A second experienced physician specializing in abdominal imaging also delineated the VOI for the same 20 patients. Observer agreement was assessed both between different raters (inter-observer) and within the same rater (intra-observer) through ICC calculations. Features with an ICC > 0.75 were selected for further analysis. Both physicians performed their assessments blinded to clinical and pathological records. Feature extraction from medical images was conducted using Pyradiomics (version 3.0.1), an open-source computational package. From both arterial and portal venous phases, 1, 502 radiomic features were derived (Supplementary Figure 1). Features were labeled with an "A" (arterial) or "V" (venous) prefix and merged using a pre-fusion approach, resulting in 3, 004 radiomic features per patient.

Radiomics feature selection, clinicalradiomics model construction, and evaluation

A 7:3 random split was used to divide HCC patients into training and validation datasets. Univariate analysis was conducted on the clinical data from the training set, and variables with P < 0.1 were included in a multivariate logistic regression to develop a clinical model. For feature dimensionality reduction, statistically insignificant features were initially excluded using t-tests (P < 0.05), followed by LASSO regression with 10-fold cross-validation. The λ value was selected based on the minimum criterion to identify the most predictive radiomic features.

After evaluating multiple machine learning-derived radiomics models, the highest-performing model was enhanced by incorporating independent prognostic factors to develop a combined model. The predictive model's calibration was assessed through (1) the generation of calibration curves comparing predicted values with actual TLSs expression, and (2) the computation of SHAP values to explain feature contributions. The model's goodness of fit was evaluated using the Hosmer-Lemeshow test. Clinical applicability was assessed via decision curve analysis (DCA).



Statistical analysis

We analyzed the data using SPSS version 27.0 (IBM Corporation). A p-value < 0.05 was considered statistically significant. For qualitative data, we applied the chi-square test and Fisher's exact test. Quantitative variables with a normal distribution were analyzed using the t-test, and results were presented as mean \pm standard deviation. For data not normally distributed, we used the rank sum test and reported results as median (interquartile range). High-dimensional feature selection, model construction, and evaluation—including LASSO regression, cross-validation, and machine learning methods—along with model interpretability analysis (SHAP analysis), were performed using Python version 3.9.

Results

Clinical characteristics

The study included 171 HCC patients, with 119 (69.6%) in the training set and 52 (30.4%) in the validation set. The prevalence of intratumoral TLSs was balanced between the two sets, with 52.94% (63/119) TLSs-positive cases in the training set and 53.85% (28/52) in the validation set (P = 0.914 for inter-set difference).

Notably, TLSs-positive patients demonstrated significantly more favorable clinical profiles (Table 1).

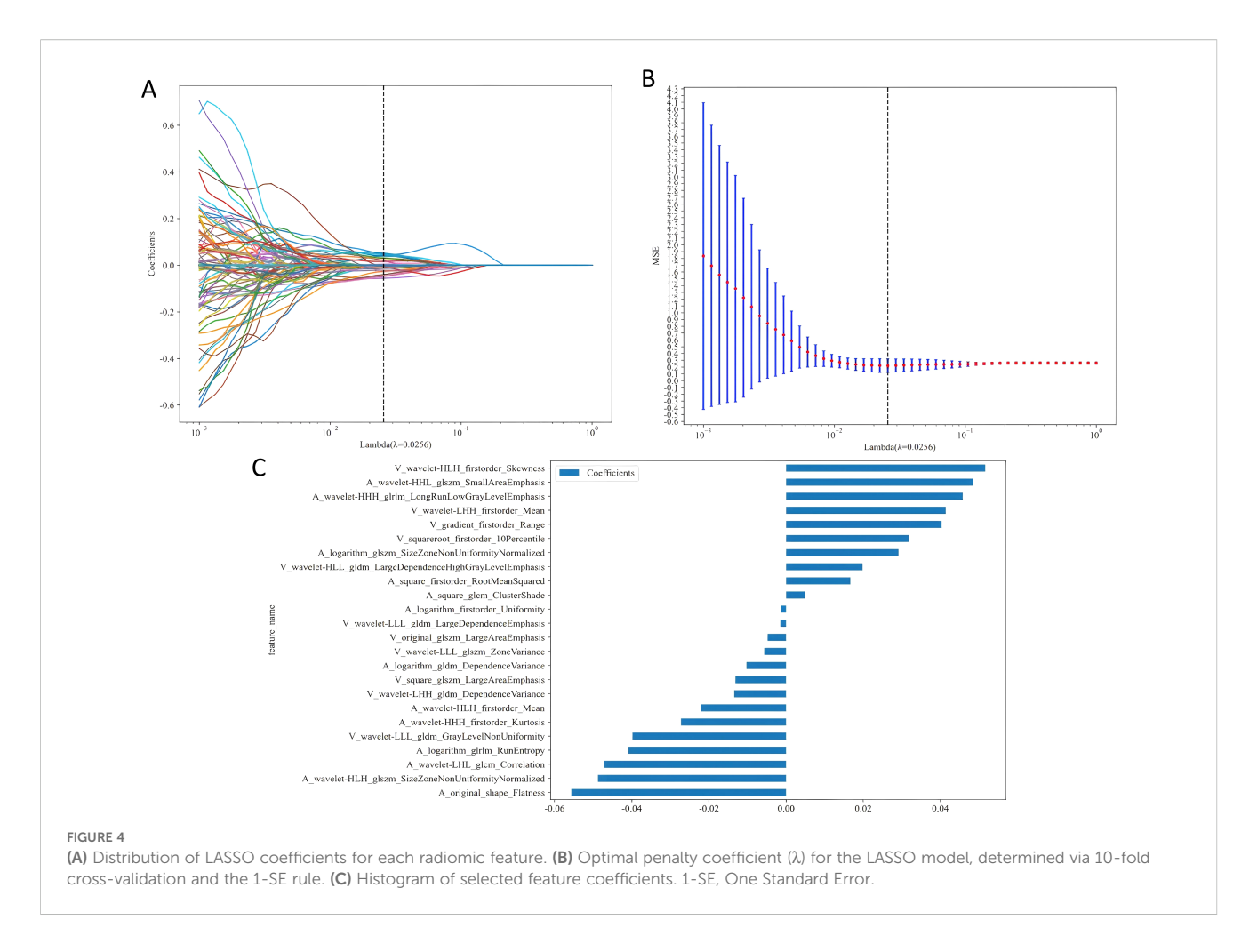
Lower rates of AFP \geq 400 ng/mL (training set: P = 0.027; validation set: P = 0.035).

Reduced prevalence of ALBI grade ≥ 2 (training set: P < 0.001; validation set: P = 0.008).

Multivariate analysis, including all variables that were significant in univariate analysis (P < 0.1), confirmed that an ALBI grade ≥ 2 is an independent negative predictor of intratumoral TLSs expression (adjusted OR: 0.32, 95% CI: 0.18–0.56; P < 0.001). Detailed results are presented in Supplementary Table 1.

Feature selection and predictive performance assessment in radiomics modeling

Our radiomics feature selection process demonstrated high reproducibility, with 94.8% (2, 847/3, 004) and 87.4% (2, 626/3, 004) of features meeting the consistency threshold (ICC \geq 0.75) in intra- and inter-observer analyses, respectively (Figures 3A, B). Ultimately, 2, 588 imaging features were retained for subsequent analysis. These features underwent rigorous statistical refinement: initial univariate screening using t-tests identified significantly



discriminative features (Figure 3C), which were then standardized and processed via LASSO regression with 10-fold cross-validation (Figures 4A, B). Following final dimensionality reduction, 24 optimal predictive radiomics features were selected (13 from the arterial phase and 11 from the portal venous phase; Figure 4C). These features were significantly correlated with the expression of intratumoral TLSs in hepatocellular carcinoma.

Building and utilizing clinical-radiomics prediction models

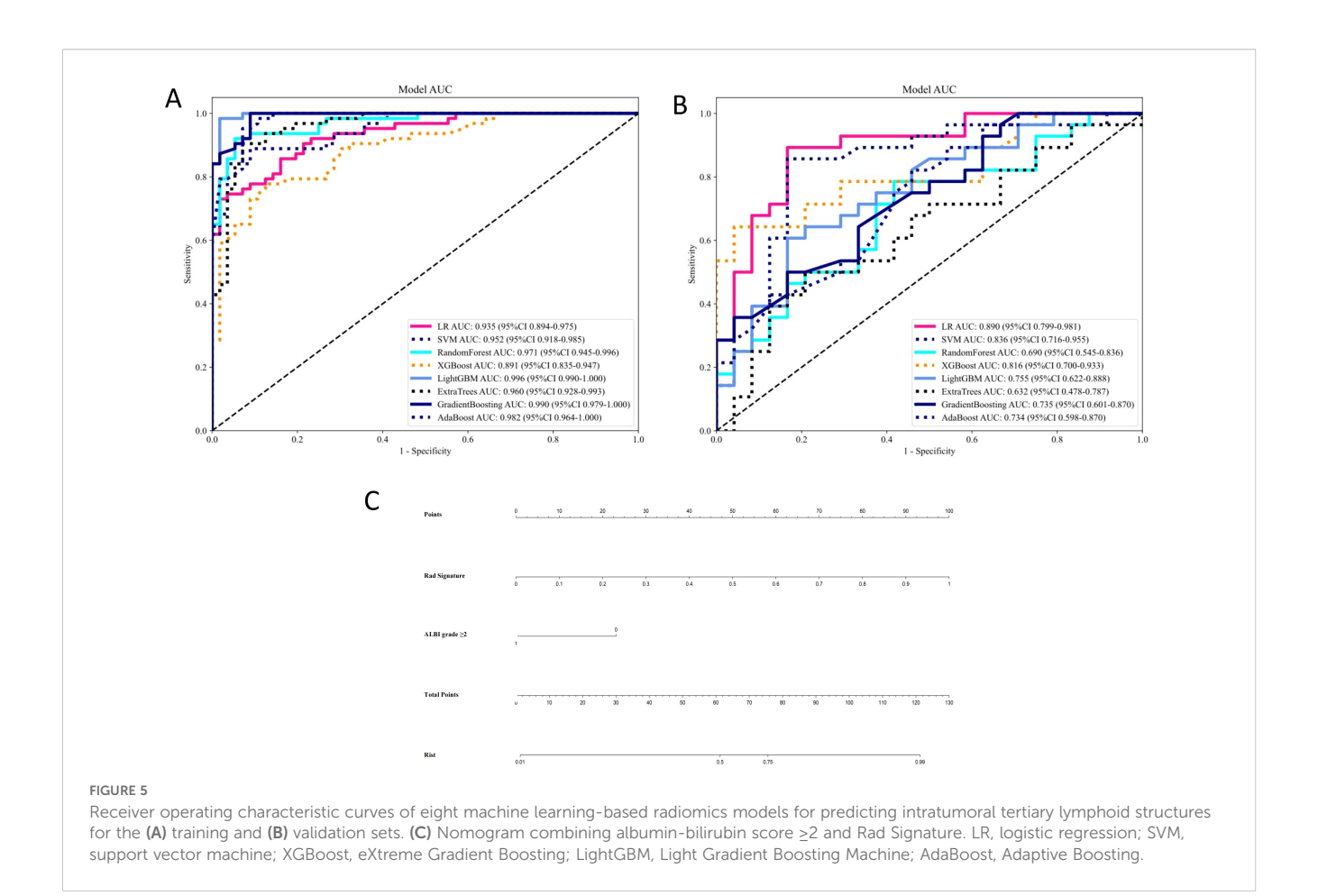
Our comprehensive evaluation of eight machine learning algorithms identified logistic regression as the optimal radiomics model, demonstrating superior predictive performance in both the training set (AUC 0.935, 95% CI 0.894–0.975) and the validation set (AUC 0.890, 95% CI 0.799–0.981) (Figures 5A, B, Table 2). SHAP analysis provided transparent interpretation of feature contributions (Figure 6), with detailed local explanations available through waterfall and force plots (Supplementary Figures 2). The integration of radiomic features with clinical predictors (ALBI grade \geq 2) in our combined nomogram (Figure 5C) achieved outstanding discrimination, with AUCs of 0.947 (95% CI 0.910–0.983) in the training set and 0.909 (95% CI 0.820–0.999) in the validation set—

representing significant improvements over the clinical-only model's performance (training AUC 0.709, validation AUC 0.714; Figures 7A, B). The model's clinical utility was further supported by excellent calibration (Figures 7C, D) and favorable decision curve analysis results (Supplementary Figure 3), confirming its reliability for predicting intratumoral TLSs expression in HCC patients.

Discussion

Surgical resection, liver transplantation, and transarterial chemoembolization (TACE) remain cornerstone treatments for HCC; however, their efficacy is often limited in advanced-stage disease (32). Accumulating evidence highlights intratumoral immune cell infiltration as a key predictor of immunotherapy response (33), with intratumoral TLSs playing a particularly critical role. The density of TLSs correlates with improved pathological responses and prolonged recurrence-free survival. Notably, the presence of atypical TLSs in tumor regression zones may promote T-cell memory formation, further underscoring their importance in HCC immunotherapy (34).

The formation of TLS alters the spatial architecture within liver cancer tumors. For instance, texture features may reflect the microscopic complexity resulting from lymphocyte aggregation,



while morphological features may correspond to the overall macroscopic structure of TLS. Although these microscopic changes are not directly visible to the naked eye in imaging, they can be decoded using quantitative radiomics algorithms. Therefore, this study employs machine learning to investigate the correlation between radiomics features of HCC and the pathological characteristics of TLS. By integrating radiomics features with clinical data, we aim to conduct an in-depth exploration of the intrinsic relationship between intratumoral TLS and HCC progression.

Our research found that the occurrence rate of intratumora TLSs among tumor cells in HCC (53.22%, 91/171) was consistent with previously reported rates (29, 35). Multivariate analysis indicated that the ALBI score was the only clinical parameter independently associated with the presence of TLSs within the tumor. The study confirmed that the ALBI score has an independent prognostic role in HCC. A higher ALBI score (2 or 3 points, compared to 1 point) independently indicates a threefold increase in the risk of death (36). Moreover, a higher ALBI score is associated with an increased risk of postoperative recurrence (37), which may reflect impaired immune surveillance in decompensated liver disease. Our data show a significant negative correlation between the ALBI score and the density of TLSs within the tumor (p < 0.05). Better liver function (lower ALBI score) may imply healthier immune system function, supporting a more effective anti-tumor immune response and the formation of TLSs. Conversely, liver dysfunction may hinder the

generation and maintenance of TLSs through systemic inflammation or immunosuppressive states. Patients with ALBI grade 1 have better immune function, promoting the generation of intratumoral TLSs and a better prognosis.

ML has emerged as a transformative tool in the medical field, demonstrating remarkable potential in various omics domains of liver cancer (26). Its application in liver cancer diagnosis is particularly prominent. Gao et al. developed an ML model that utilizes preoperative contrast-enhanced CT imaging and clinical data to distinguish malignant liver tumors. The model achieved an accuracy rate of 86.2% and an AUC value of 0.893, enabling the differentiation between HCC and intrahepatic cholangiocarcinoma (ICC) (38).

ML also exhibits outstanding practicality in predicting key histopathological features of liver cancer. MVI, an important predictor of postoperative recurrence, has long been a focus of radiomics research. Multiple ML models incorporating radiomics features have demonstrated excellent performance in predicting MVI (39, 40). These advancements highlight the ability of machine learning to extract clinically relevant information from routine imaging data, indicating that ML can obtain certain pathological features of tumors from imaging materials.

To date, no studies have developed ML models combining CT radiomics and clinical data to predict intratumoral TLSs expression in HCC. However, pioneering work by Xu et al. demonstrated ML's

TABLE 1 Characteristics of patients in the training and validation sets.

| | Training set (n=119) | | | Validation set (n=52) | | |
|--|---|------------------------|-------|-------------------------|-------------------------|-------|
| Variables | TLSs-negative TLSs-positive (n=56) (n=63) | | Р | TLSs-negative (n=24) | TLSs-positive (n=28) | Р |
| Age (y), mean ± SD | 58.57 ± 9.66 | 59.29 ± 9.51 | 0.686 | 57.38 ± 10.11 | 58.64 ± 9.63 | 0.646 |
| WBC (×10 ⁹ /L), M (Q ₁ , Q ₃) | 5.00 (3.80, 5.73) | 4.60 (3.70, 6.70) | 0.617 | 5.45 (4.77, 6.73) | 5.50 (4.40, 6.65) | 0.776 |
| RBC (×10 ¹² /L), M (Q ₁ , Q ₃) | 4.47 (4.00, 4.77) | 4.44 (4.08, 4.71) | 0.964 | 4.61 (4.20, 4.81) | 4.42 (4.04, 4.75) | 0.287 |
| PLT (×10 ⁹ /L), M (Q ₁ , Q ₃) | 144.00 (115.50, 169.50) | 153.00 (95.00, 224.00) | 0.239 | 163.50 (146.75, 197.00) | 164.00 (134.00, 216.00) | 0.640 |
| ALT (U/L), M (Q ₁ , Q ₃) | 34.28 (24.00, 47.18) | 28.72 (22.77, 42.52) | 0.270 | 38.56 (20.88, 44.39) | 26.60 (18.14, 39.15) | 0.204 |
| AST (U/L), M (Q ₁ , Q ₃) | 32.00 (23.75, 45.75) | 27.83 (21.02, 40.86) | 0.322 | 24.76 (19.84, 34.82) | 28.78 (22.62, 41.89) | 0.162 |
| PT (s), M (Q ₁ , Q ₃) | 13.90 (13.40, 14.50) | 13.90 (13.40, 14.45) | 0.784 | 13.60 (12.97, 13.90) | 13.70 (13.20, 14.30) | 0.398 |
| APTT (s), M (Q ₁ , Q ₃) | 35.60 (34.35, 37.80) | 36.60 (34.90, 39.40) | 0.221 | 37.45 (34.88, 38.68) | 35.45 (34.03, 38.28) | 0.169 |
| Sex, n (%) | | | 0.828 | | | 0.359 |
| Male | 86 (72.27) | 41 (73.21) | | 38 (73.08) | 19 (79.17) | |
| Female | 33 (27.73) | 15 (26.79) | | 14 (26.92) | 5 (20.83) | |
| HBV/HCV, n (%) | | | 0.939 | | | 1.000 |
| Negative | 28 (23.53) | 13 (23.21) | | 10 (19.23) | 5 (20.83) | |
| Positive | 91 (76.47) | 43 (76.79) | | 42 (80.77) | 19 (79.17) | |
| Liver cirrhosis, n (%) | | | 0.500 | | | 0.111 |
| Negative | 76 (63.87) | 34 (60.71) | | 38 (73.08) | 15 (62.50) | |
| Positive | 43 (36.13) | 22 (39.29) | | 14 (26.92) | 9 (37.50) | |
| BCLC, n (%) | | | 0.435 | | | 0.882 |
| 0-A | 95 (79.83) | 43 (76.79) | | 44 (84.62) | 21 (87.50) | |
| В | 24 (20.17) | 13 (23.21) | | 8 (15.38) | 3 (12.50) | |
| AFP≥400ng/ml, n (%) | | | 0.027 | | | 0.013 |
| Negative | 78 (65.55) | 31 (55.36) | | 27 (51.92) | 8 (33.33) | |
| Positive | 41 (34.45) | 25 (44.64) | | 25 (48.08) | 16 (66.67) | |
| ALBI grade≥2, n (%) | | | <.001 | | | <.001 |
| Negative | 54 (45.38) | 11 (19.64) | | 25 (48.08) | 5 (20.83) | |
| Positive | 65 (54.62) | 45 (80.36) | | 27 (51.92) | 19 (79.17) | |

Data are presented as number (%), median (interquartile range), or mean \pm SD.

SD, standard deviation; WBC, white blood cell; RBC, red blood cell; PLT, platelets; ALT, alanine aminotransferase; AST, aspartate aminotransferase; PT, prothrombin time; APTT, activated partial thromboplastin time; HBV, hepatitis B virus; HCV, hepatitis C virus; BCLC, Barcelona Clinic Liver Cancer Staging System; AFP, alpha-fetoprotein; ALBI, albumin-bilirubin. The bold values represents a statistically significant difference.

capability to predict TLSs in intrahepatic cholangiocarcinoma (ICC) using preoperative contrast-enhanced CT portal phase and multiphase MRI images (41). Subsequent research expanded on this approach, employing multiphase MRI and clinical data from 192 patients to predict intratumoral TLSs in ICC (42). For HCC specifically, prior investigations have utilized contrast-enhanced CT semantic features combined with clinical data to predict intratumoral TLSs patterns, achieving an average AUC of 0.75 through five-fold cross-validation (43). These foundational studies not only validate our methodological approach but also confirm the feasibility of preoperative TLSs prediction. However, a recent study focused on the density of the peritumoral TLS (pTLS) around the

tumors of HCC patients and their role in predicting prognosis and immune treatment response. By integrating multi-omics data (including spatial transcriptomics and RNA sequencing) and multi-center imaging data, the study identified key regulatory factors (CXCL9/10) associated with high pTLS density and developed a non-invasive classifier based on MRI imaging biomarkers to accurately predict the density of pTLS (44).

Our study represents the first successful development of machine learning models that integrate contrast-enhanced CT radiomics with clinical parameters to predict intratumoral TLSs expression in HCC. While our clinical-only model achieved comparable performance (AUC ≈ 0.75) to previous HCC studies,

TABLE 2 Diagnostic performance of eight machine learning models in the training and validation sets.

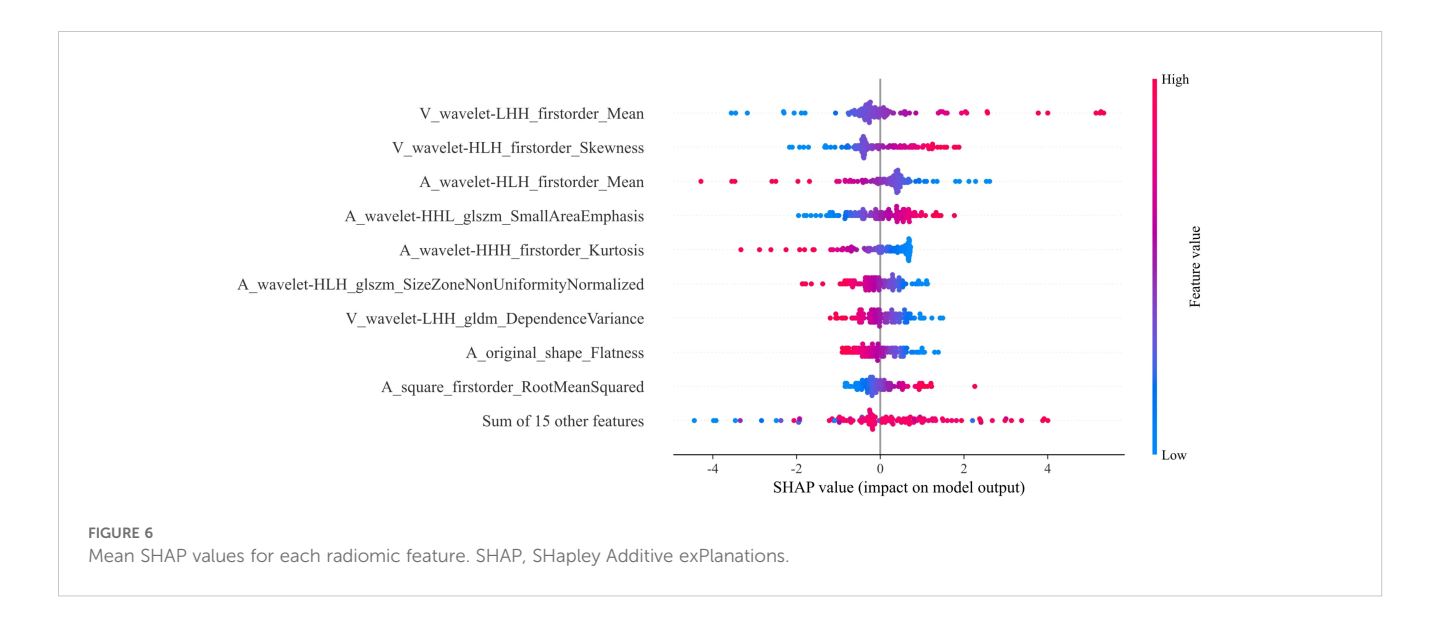
| Set | Model | Accuracy | Sensitivity | Specificity | AUC (95% CI) |
|------------|------------------|----------|-------------|-------------|------------------|
| Training | LR | 0.84 | 0.71 | 0.98 | 0.93 (0.78-0.98) |
| | SVM | 0.89 | 0.83 | 0.96 | 0.95 (0.92-0.98) |
| | RandomForest | 0.92 | 0.90 | 0.95 | 0.97 (0.95–1.00) |
| | XGBoost | 0.82 | 0.76 | 0.87 | 0.89 (0.83-0.95) |
| | LightGBM | 0.97 | 0.97 | 0.98 | 1.00 (0.99-1.00) |
| | ExtraTrees | 0.90 | 0.87 | 0.93 | 0.96 (0.92-0.99) |
| | GradientBoosting | 0.93 | 0.95 | 0.91 | 0.99 (0.97–1.00) |
| | AdaBoost | 0.92 | 0.92 | 0.93 | 0.98 (0.96–1.00) |
| Validation | LR | 0.85 | 0.86 | 0.83 | 0.89 (0.80-0.98) |
| | SVM | 0.83 | 0.82 | 0.83 | 0.84 (0.72-0.95) |
| | RandomForest | 0.67 | 0.75 | 0.58 | 0.69 (0.55-0.84) |
| | XGBoost | 0.77 | 0.61 | 0.96 | 0.82 (0.70-0.93) |
| | LightGBM | 0.69 | 0.57 | 0.83 | 0.76 (0.62-0.89) |
| | ExtraTrees | 0.62 | 0.46 | 0.79 | 0.63 (0.48-0.79) |
| | GradientBoosting | 0.63 | 0.46 | 0.83 | 0.74 (0.60-0.87) |
| | AdaBoost | 0.67 | 0.79 | 0.54 | 0.73 (0.60-0.87) |

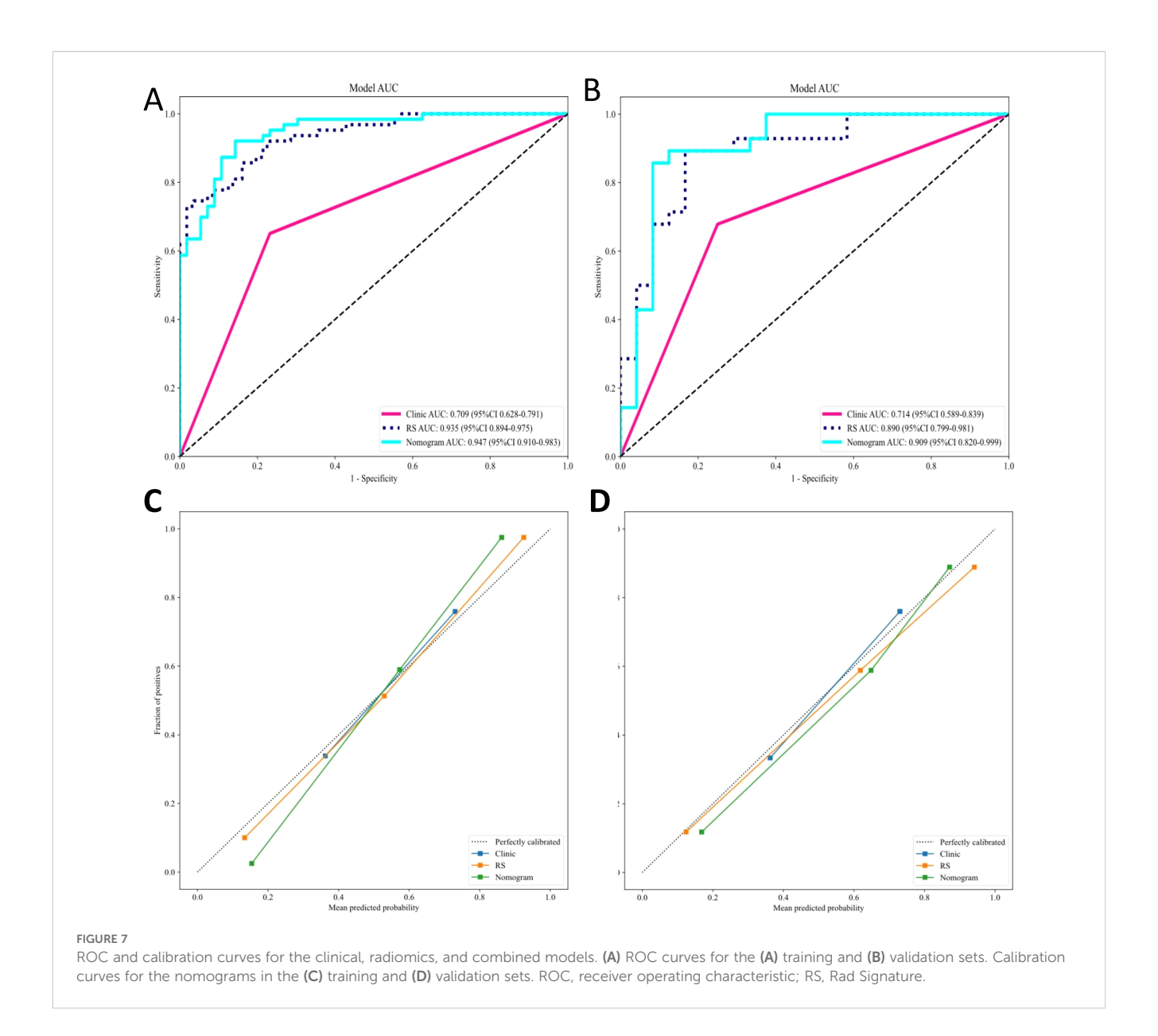
AUC, area under the curve; ACC; LR, logistic regression; SVM, support vector machine; XGBoost, eXtreme Gradient Boosting; LightGBM, Light Gradient Boosting Machine; AdaBoost, Adaptive Boosting,

the radiomics model and combined model demonstrated significantly superior predictive capability, with the integrated nomogram (combining ALBI score and radiomic features) emerging as the optimal tool for preope.

This study has several limitations that should be considered. First, the retrospective design may introduce selection bias, and since our inclusion criteria were restricted to surgical patients, the findings are currently only applicable to resectable HCC cases - additional studies

are needed to evaluate generalizability to advanced/unresectable HCC populations. Second, as a single-center retrospective analysis, external validation through prospective multicenter trials will be essential to confirm our results and support clinical translation. Third, while our radiomics model demonstrated promising results using contrastenhanced CT alone, incorporating preoperative MRI in future studies could further improve predictive performance and provide stronger evidence for clinical implementation through multimodal





imaging integration. Finally, due to the retrospective nature of this study, we were unable to prepare traditional clear pathological section images. Although we have made every effort to provide detailed textual descriptions, this deficiency still exists. In future related studies, attention should be paid to the collection and presentation of pathological images. In the future, we will continue to increase the number of patients. We will also analyze the relationship between the presence of TLSs and the prognosis of HCC patients and verify its correlation with the efficacy of immunotherapy. At the same time, we may explore the connections between imaging features such as MRI and PET-CT and TLSs in HCC patients. The integrated model constructed in this study aims to become a highly accurate, noninvasive "virtual biopsy" tool, which not only can guide the clinical decision-making of immunotherapy for patients with hepatocellular carcinoma but also will promote the exploration of the underlying mechanisms of the tumor immune microenvironment.

Conclusion

In summary, the developed machine learning models for preoperative prediction of intratumoral TLSs expression in HCC by integrating radiomic features extracted from arterial and portal phase contrast-enhanced CT images with relevant clinical data. Our models - including clinical-only, radiomics-only, and combined approaches - consistently demonstrated robust predictive performance across both training and validation sets. These findings suggest that our ML framework could serve as a valuable clinical tool for noninvasive intratumoral TLSs assessment prior to surgery, potentially guiding personalized treatment selection and optimizing therapeutic decision-making for HCC patients. The strong performance across all model types highlights the complementary value of both imaging biomarkers and clinical parameters in predicting this important immunological feature of HCC.

Data availability statement

The raw data supporting the conclusions of this article will be made available by the authors, without undue reservation.

Ethics statement

The studies involving humans were approved by The Ethics Committee of Northern Theater General Hospital. The studies were conducted in accordance with the local legislation and institutional requirements. The ethics committee/institutional review board waived the requirement of written informed consent for participation from the participants or the participants' legal guardians/next of kin because This retrospective study has anonymized patient data and does not impact patients in any way.

Author contributions

JW: Writing – original draft, Writing – review & editing. ZfZ: Investigation, Writing – review & editing. LN: Writing – review & editing. WZ: Methodology, Writing – review & editing. YG: Data curation, Writing – review & editing. ZwZ: Software, Writing – review & editing. QYR: Data curation, Writing – review & editing. WKP: Writing – original draft, Writing – review & editing. LH: Writing – original draft, Writing – review & editing.

Funding

The author(s) declare financial support was received for the research and/or publication of this article. The research work and publication of this article were funded by the 2024 Liaoning Provincial Joint Research Project of Science and Technology (Project Number: 2024JH2/102600291).

References

- 1. Llovet JM, Kelley RK, Villanueva A, Singal AG, Pikarsky E, Roayaie S, et al. Hepatocellular carcinoma. *Nat Rev Dis Primers.* (2021) 7:6. doi: 10.1038/s41572-020-00240-3
- 2. Bray F, Laversanne M, Sung H, Ferlay J, Siegel RL, Soerjomataram I, et al. Global cancer statistics 2022: GLOBOCAN estimates of incidence and mortality worldwide for 36 cancers in 185 countries. *CA Cancer J Clin*. (2024) 74:229–63. doi: 10.3322/caac.21834
- Li H, Meng L, Yu S, Zheng H, Yu L, Wang H, et al. Efficacy and safety of robotic versus laparoscopic liver resection for hepatocellular carcinoma: a propensity score-matched retrospective cohort study. Hepatol Int. (2024) 18:1271–85. doi: 10.1007/s12072-024-10658-6
- 4. Yang X, Xu H, Zuo B, Yang X, Bian J, Long J, et al. Downstaging and resection of hepatocellular carcinoma in patients with extrahepatic metastases after stereotactic therapy. *Hepatobiliary Surg Nutr.* (2021) 10:434–42. doi: 10.21037/hbsn-21-188
- 5. Machairas N, Tsilimigras DI, Pawlik TM. State-of-the-art surgery for hepatocellular carcinoma. *Langenbecks Arch Surg.* (2021) 406:2151–62. doi: 10.1007/s00423-021-02298-3
- 6. Zou Y, Wan X, Zhou Q, Zhu G, Lin S, Tang Q, et al. Mechanisms of drug resistance in hepatocellular carcinoma. *Biol Proced Online*. (2025) 27:19. doi: 10.1186/s12575-025-00281-6
- 7. Ho WJ, Zhu Q, Durham J, Popovic A, Xavier S, Leatherman J, et al. Neoadjuvant cabozantinib and nivolumab converts locally advanced HCC into resectable disease

Conflict of interest

The authors declare that the research was conducted in the absence of any commercial or financial relationships that could be construed as a potential conflict of interest.

Generative AI statement

The authors declare that no Gen AI was used in the creation of this manuscript.

Any alternative text (alt text) provided alongside figures in this article has been generated by Frontiers with the support of artificial intelligence and reasonable efforts have been made to ensure accuracy, including review by the authors wherever possible. If you identify any issues, please contact us.

Publisher's note

All claims expressed in this article are solely those of the authors and do not necessarily represent those of their affiliated organizations, or those of the publisher, the editors and the reviewers. Any product that may be evaluated in this article, or claim that may be made by its manufacturer, is not guaranteed or endorsed by the publisher.

Supplementary material

The Supplementary Material for this article can be found online at: https://www.frontiersin.org/articles/10.3389/fonc.2025.1652509/full#supplementary-material

- with enhanced antitumor immunity. Nat Cancer. (2021) 2:891-903. doi: 10.1038/s43018-021-00234-4
- 8. Zhu XD, Huang C, Shen YH, Xu B, Ge NL, Ji Y, et al. Hepatectomy after conversion therapy using tyrosine kinase inhibitors plus anti-PD-1 antibody therapy for patients with unresectable hepatocellular carcinoma. *Ann Surg Oncol.* (2023) 30:2782–90. doi: 10.1245/s10434-022-12530-z
- 9. Yau T, Park JW, Finn RS, Cheng AL, Mathurin P, Edeline J, et al. Nivolumab versus sorafenib in advanced hepatocellular carcinoma (CheckMate 459): a randomised, multicentre, open-label, phase 3 trial. *Lancet Oncol.* (2022) 23:77–90. doi: 10.1016/S1470-2045(21)00604-5
- 10. Finn RS, Zhu AX. Evolution of systemic therapy for hepatocellular carcinoma. Hepatology. (2021) 73:150–7. doi: 10.1002/hep.31306
- 11. Li X, Chu X, Xu W, Yang Y, Wei T, Bo Y, et al. Integrated spatial transcriptomic profiling to dissect the cellular characteristics of tumor-associated tertiary lymphoid structures. *Cell Rep.* (2025) 44:116250. doi: 10.1016/j.celrep.2025.116250
- 12. Dieu-Nosjean MC, Giraldo NA, Kaplon H, Germain C, Fridman WH. Tertiary lymphoid structures, drivers of the anti-tumor responses in human cancers. *Immunol Rev.* (2016) 271:260–75. doi: 10.1111/imr.12405
- 13. Schumacher TN, Thommen DS. Tertiary lymphoid structures in cancer. *Science*. (2022) 375:eabf9419. doi: 10.1126/science.abf9419

- 14. Li H, Wang J, Liu H, Lan T, Xu L, Wang G, et al. Existence of intratumoral tertiary lymphoid structures is associated with immune cells infiltration and predicts better prognosis in early-stage hepatocellular carcinoma. *Aging (Albany NY)*. (2020) 12:3451–72. doi: 10.18632/aging.102821
- 15. Cabrita R, Lauss M, Sanna A, Donia M, Skaarup Larsen M, Mitra S, et al. Tertiary lymphoid structures improve immunotherapy and survival in melanoma. *Nature*. (2020) 577:561–5. doi: 10.1038/s41586-019-1914-8
- 16. Vanhersecke L, Brunet M, Guégan JP, Rey C, Bougouin A, Cousin S, et al. Mature tertiary lymphoid structures predict immune checkpoint inhibitor efficacy in solid tumors independently of PD-L1 expression. *Nat Cancer*. (2021) 2:794–802. doi: 10.1038/s43018-021-00232-6
- 17. Petitprez F, de Reyniès A, Keung EZ, Chen TW, Sun CM, Calderaro J, et al. B cells are associated with survival and immunotherapy response in sarcoma. *Nature*. (2020) 577:556–60. doi: 10.1038/s41586-019-1906-8
- 18. Xie Y, Peng H, Hu Y, Jia K, Yuan J, Liu D, et al. Immune microenvironment spatial landscapes of tertiary lymphoid structures in gastric cancer. *BMC Med.* (2025) 23:59. doi: 10.1186/s12916-025-03889-3
- 19. Gunderson J, Rajamanickam V, Bui C, Bernard B, Pucilowska J, Ballesteros-Merino C, et al. Germinal center reactions in tertiary lymphoid structures associate with neoantigen burden, humoral immunity and long-term survivorship in pancreatic cancer. *Oncoimmunology*. (2021) 10:1900635. doi: 10.1080/2162402X.2021.1900635
- 20. Zhang Y, Li J, Yang F, Zhang X, Ren X, Wei F. Relationship and prognostic significance of IL-33, PD-1/PD-L1, and tertiary lymphoid structures in cervical cancer. *J Leukoc Biol.* (2022) 112:1591–603. doi: 10.1002/JLB.5MA0322-746R
- 21. Zhang K, Xie X, Zou LH, Guo SQ. Tertiary lymphoid structures are associated with a favorable prognosis in high-grade serous ovarian cancer patients. *Reprod Sci.* (2023) 30:2468–80. doi: 10.1007/s43032-023-01188-x
- 22. Fan X, Feng D, Wei D, Li A, Wei F, Deng S, et al. Characterizing tertiary lymphoid structures associated single-cell atlas in breast cancer patients. *Cancer Cell Int.* (2025) 25:12. doi: 10.1186/s12935-025-03635-y
- 23. Calderaro J, Petitprez F, Becht E, Laurent A, Hirsch TZ, Rousseau B, et al. Intratumoral tertiary lymphoid structures are associated with a low risk of early recurrence of hepatocellular carcinoma. *J Hepatol.* (2019) 70:58–65. doi: 10.1016/j.jhep.2018.09.003
- 24. Ding GY, Ma JQ, Yun JP, Chen X, Ling Y, Zhang S, et al. Distribution and density of tertiary lymphoid structures predict clinical outcome in intrahepatic cholangiocarcinoma. *J Hepatol.* (2022) 76:608–18. doi: 10.1016/j.jhep.2021.10.030
- 25. Bakrania A, Joshi N, Zhao X, Zheng G, Bhat M. Artificial intelligence in liver cancers: Decoding the impact of machine learning models in clinical diagnosis of primary liver cancers and liver cancer metastases. *Pharmacol Res.* (2023) 189:106706. doi: 10.1016/j.phrs.2023.106706
- 26. Calderaro J, Seraphin TP, Luedde T, Simon TG. Artificial intelligence for the prevention and clinical management of hepatocellular carcinoma. *J Hepatol.* (2022) 76:1348–61. doi: 10.1016/j.jhep.2022.01.014
- 27. Wu X, You J, Zhang S, Zhang B. Pretreatment CT-based machine learning radiomics model predicts response in unresectable hepatocellular carcinoma treated with lenvatinib plus PD-1 inhibitors and interventional therapy. *J Immunother Cancer*. (2024) 12:e010330. doi: 10.1136/jitc-2024-010330
- 28. Feng ST, Jia Y, Liao B, Huang B, Zhou Q, Li X, et al. Preoperative prediction of microvascular invasion in hepatocellular cancer: a radiomics model using Gd-EOB-DTPA-enhanced MRI. *Eur Radiol.* (2019) 29:4648–59. doi: 10.1007/s00330-018-5935-8
- 29. Li M, Fan Y, You H, Li C, Luo M, Zhou J, et al. Dual-energy CT deep learning radiomics to predict macrotrabecular-massive hepatocellular carcinoma. *Radiology*. (2023) 308:e230255. doi: 10.1148/radiol.230255

- 30. Reig M, Forner A, Rimola J, Ferrer-Fàbrega J, Burrel M, Garcia-Criado Á, et al. BCLC strategy for prognosis prediction and treatment recommendation: The 2022 update. *J Hepatol.* (2022) 76:681–93. doi: 10.1016/j.jhep.2021.11.018
- 31. Ginès P, Krag A, Abraldes JG, Solà E, Fabrellas N, Kamath PS. Liver cirrhosis. *Lancet*. (2021) 398:1359–76. doi: 10.1016/S0140-6736(21)01374-X
- 32. Yang C, Zhang H, Zhang L, Zhu AX, Bernards R, Qin W, et al. Evolving therapeutic landscape of advanced hepatocellular carcinoma. *Nat Rev Gastroenterol Hepatol.* (2023) 20:203–22. doi: 10.1038/s41575-022-00704-9
- 33. Li M, Bhoori S, Mehta N, Mazzaferro V. Immunotherapy for hepatocellular carcinoma: The next evolution in expanding access to liver transplantation. *J Hepatol.* (2024) 81:743–55. doi: 10.1016/j.jhep.2024.05.037
- 34. Shu DH, Ho WJ, Kagohara LT, Girgis A, Shin SM, Danilova L, et al. Immunotherapy response induces divergent tertiary lymphoid structure morphologies in hepatocellular carcinoma. *Nat Immunol.* (2024) 25:2110-23. doi: 10.1038/s41590-024-01992-w
- 35. Sofopoulos M, Fortis SP, Vaxevanis CK, Sotiriadou NN, Arnogiannaki N, Ardavanis A, et al. The prognostic significance of peritumoral tertiary lymphoid structures in breast cancer. *Cancer Immunol Immunother*. (2019) 68:1733–45. doi: 10.1007/s00262-019-02407-8
- 36. Fulgenzi CAM, Cheon J, D'Alessio A, Nishida N, Ang C, Marron TU, et al. Reproducible safety and efficacy of atezolizumab plus bevacizumab for HCC in clinical practice: Results of the AB-real study. *Eur J Cancer (Oxford England: 1990).* (2022) 175:204–13. doi: 10.1016/j.ejca.2022.08.024
- 37. Sun T, Wang X, Zhu G, Zhang J, Huang J, Li R, et al. The EZ-ALBI and PALBI scores contribute to the clinical application of ALBI in predicting postoperative recurrence of HCC. *Sci Rep.* (2025) 15:9132. doi: 10.1038/s41598-025-93716-9
- 38. Gao R, Zhao S, Aishanjiang K, Cai H, Wei T, Zhang Y, et al. Deep learning for differential diagnosis of Malignant hepatic tumors based on multi-phase contrast-enhanced CT and clinical data. *J Hematol Oncol.* (2021) 14:154. doi: 10.1186/s13045-021-01167-2
- 39. Han X, Shan L, Xu R, Zhou J, Lu M. Assessing MRI-based artificial intelligence models for preoperative prediction of microvascular invasion in hepatocellular carcinoma: A systematic review and meta-analysis. *Acad Radiol.* (2025) 25:S1076–6332(25)00608-7. doi: 10.1016/j.acra.2025.06.030
- 40. Yuan E, Chen Y, Song B. Quality of radiomics for predicting microvascular invasion in hepatocellular carcinoma: a systematic review. *Eur Radiol.* (2023) 33:3467–77. doi: 10.1007/s00330-023-09414-5
- 41. Xu Y, Li Z, Yang Y, Li L, Zhou Y, Ouyang J, et al. A CT-based radiomics approach to predict intra-tumoral tertiary lymphoid structures and recurrence of intrahepatic cholangiocarcinoma. *Insights Imaging*. (2023) 14:173. doi: 10.1186/s13244-023-01527-1
- 42. Xu Y, Li Z, Yang Y, Zhang Y, Li L, Zhou Y, et al. Association between MRI radiomics and intratumoral tertiary lymphoid structures in intrahepatic cholangiocarcinoma and its prognostic significance. *J Magn Reson Imaging*. (2024) 60:715–28. doi: 10.1002/jmri.29128
- 43. Li P, Liang Y, Zeng B, Yang G, Zhu C, Zhao K, et al. Preoperative prediction of intra-tumoral tertiary lymphoid structures based on CT in hepatocellular cancer. *Eur J Radiol.* (2022) 151:110309. doi: 10.1016/j.ejrad.2022.110309
- 44. Long S, Li M, Chen J, Zhong L, Abudulimu A, Zhou L, et al. Spatial patterns and MRI-based radiomic prediction of high peritumoral tertiary lymphoid structure density in hepatocellular carcinoma: a multicenter study. *J Immunother Cancer*. (2024) 12: e009879. doi: 10.1136/jitc-2024-009879